Electrocatalytic hydrogen evolution performance of mesoporous Ni/NiO/carbon composites fabricated from carbon dots

Yan Yang, Ruihan Liu, Weiruo Liu, Lexuan Ji, Mengjie Gao, Yunpu Zhai*

College of Chemistry, Zhengzhou University, 100 Kexue Avenue, Zhengzhou 450001, Henan, PR China

* Corresponding author.

E-mail address: yunpu.zhai@zzu.edu.cn

Abstract

Mesoporous Ni/NiO/carbon composites were successfully prepared from the tri-component self-assembly of carbon dots, nickel precursors and surfactant F127. The functional groups of carbon dots can chelate with the metal and then further assemble with the surfactant to prepare mesoporous metals/carbon materials (Ni-NC/MC), which are applied to the electrolysis of water to produce hydrogen. The results show that the interaction between Ni/NiO heterostructures is the active component of the catalyst. The carbon dots show a certain confinement effect, which hinders the further growth of metal particles. Moreover, large specific surface area and suitable Ni/NiO ratio are beneficial to the HER catalytic activity and operational stability of the catalyst.

Key Words: Carbon dot; mesoporous carbon; nickel; hydrogen evolution reaction; electrocatalyst

1 Introduction

In the contemporary world, the energy crisis and climate problems have become increasingly serious, stimulating the development of alternative scenarios and renewable energy supply. Compared with traditional energy sources, hydrogen is rich in resources and has high calorific value. The combustion products do not cause any

pollution to the environment, and it is obtained by electrolysis with water as raw material. However, the further application of hydrogen production by electrochemical water splitting into electrolytic cells is mainly hindered by the slow kinetic process of hydrogen evolution reaction (HER) and oxygen evolution reaction (OER), which requires efficient catalysts to accelerate the reaction and improve the reaction efficiency.[1-5]It has been proved that efficient catalysts should have high electrocatalytic activity for electron transfer and a highly porous structure that facilitates transport.[6]

Noble metal (Pt, Ru, Ir)-based electrocatalysts are currently considered to be the most active materials for hydrogen evolution reaction (HER), which have high intrinsic electrocatalytic activity and can be effectively combined with other materials to obtain superior catalytic performance. However, in the process of HER reaction, noble metal-based catalysts have the problems of high cost, easy agglomeration and poor stability, which seriously limits the development and application of noble metal-based catalysts.[7] Therefore, people are focusing on the development of efficient, durable and cost-effective non-precious metal electrocatalysts, including transition metal alloys, phosphides, nitrides, sulfides, carbides and nano-carbon-based materials, etc.[8-11] Among them, nickel is considered to be a promising HER candidate due to its unoccupied *d* orbital and unpaired *d* electrons, which exhibits good HER activity, suitable price, and high conductivity.[12, 13] However, the disadvantages such as poor stability limit their wide application. Therefore, researchers have designed various schemes to improve the activity of the catalyst, such as designing special nanostructures to expose more active sites, adding conductive substrates, increasing overall conductivity, doping atoms to optimize the electronic structure of the active center, and electrochemical activation to construct new active phases, etc.[14, 15]

Carbon materials, with their advantages of low cost, adjustable element doping, high conductivity, and good chemical stability, have become promising electrode materials with high durability.[6, 16] Doping heteroatoms onto carbon substrates can affect the distribution of electrons in adjacent carbon atoms due to the different electronegativities between the heteroatoms and carbon atoms, leading to alterations in the adsorption capability and catalytic activity of carbon in reaction systems.[17] Among

them, nitrogen doping is one of the most widely studied materials because it allows surface modification of carbon as well as structural optimization. Due to electronegativity differences and charge polarization, nitrogen doping generally exhibits stronger hydrophilicity and stronger guest-host interactions, while improving the conductivity of the carbon skeleton.[18] Carbon dots (CDs) are carbon particles with a size less than 10 nm. They are typically prepared by hydrothermal treatment of organic precursors. Different doping elements can be introduced by adjusting the precursor type. CDs are rich in surface functional groups, which can chelate with metals. This enables CDs and metals to be used as basic building blocks for subsequent assembly and transformation, while avoiding metal aggregation.[19] In an earlier report, Song et al. designed sea urchin-like F-CDs/CoP as a bifunctional catalyst, which provided a low cell voltage of 1.48 V to drive overall water decomposition at a current density of 10 mA cm^{-2}.[19] Hong et al. inserted CDs in situ into cobalt-based zeolite imidazolate framework (Co-ZIF) nanosheet arrays (Co-ZIF/CDs/CC) requiring only an overpotential of 226 mV to deliver 10 mA cm^{-2} in 1.0 M KOH.[20] Purbia et al. recently reported a Cu single-atom-modified N-doped carbon dots (Cu-SACs-N-CQDs) brought extremely high Faraday efficiency (> 80%).[21] Currently, carbon dots and metals present a more dense sheet-like structure after roasting, which is not favorable to the exposure of active sites and the penetration of electrolytes.[22] Therefore, if pores are introduced, it is beneficial to increase the active specific surface area of the electrode and the utilization of the active sites, and provide more channels for the transport of electrolytes, reactants and products, while such work is less reported at present.

In this paper, the rich functional groups on the surface of carbon dots are used to drive the synergistic assembly of metals and surfactants. At the same time, the size effect of carbon dots is used to limit the further growth of metals, and metal nanoparticles supported on nitrogen-doped carbon substrates are synthesized (Ni-NC/MC). The incorporation of heteroatoms and the large specific surface area exposed more active sites, which enhanced the material transport during the reaction, and the graphitization characteristics made the catalyst have good electrical conductivity and mechanical strength.[23, 24] The metal mainly existed in the form of Ni/NiO. By

comparing the electrocatalytic performance of the catalyst for HER in alkaline electrolyte. The promotion effect of pore and carbon dot size effect on electrochemical performance was verified.

2 Experimental sections

2.1 Materials

L-tryptophan (AR), anhydrous citric acid (AR) and potassium hydroxide (AR) were bought from Aldrich Chemical Co. Pluronic F127, nickel nitrate hexahydrate (AR) were bought from Xilong Science Co. All chemicals were used without further purification.

2.2 Characterization

The morphology, microstructure and composition of the catalyst were characterised by scanning electron microscopy (SEM, ZEISS Gemini 300), transmission electron microscopy (TEM, FEI's Talos-F200S), CT tomography X-ray diffraction system (XRD, Panaco Empyrean) and X-ray photoelectron spectroscopy (XPS, Esca Lab Xi+). The SEM used an energy spectrometer model, OXFORD XPLORE 30, with an AuPd alloy as the gold target. For XRD, a Cu target material was utilized, with a working voltage of 45 kV and working current of 40 mA. The scanning range is from 5 to 80 °, with a step length of 0.013 ° and residence time of 10.2 s. The specific surface area and pore size distribution of the catalyst were measured using the ASAP2420-4MP automatic physical adsorption instrument from Micromeritic. The specific surface area of the catalyst was calculated by the Brunauer-Emmett-Teller (BET) method. The pore size distribution was calculated by the Barrett-Joyner-Halenda (BJH) method. Nitrogen content was measured by Flash EA 1112m from Thermo, USA. The Inductively Coupled Plasma Atomic Emission Spectrometry (ICP-OES, Agilent 5110 series) was utilized to determine the weight percentage of metals present in the catalyst sample. The Raman spectrum was collected using the Lab RAM HR Evo Raman spectrometer manufactured by HORIBA, France, using green light (514 nm) as the excitation source.

2.3 Synthesis of NCDs

Citric acid (6.73 g) and 7.15 g of tryptophan were dissolved in 70 ml of water. The mixed solution was placed in a polytetrafluoroethylene-lined reactor at 180 °C for 5h. The solution was freeze-dried after cooling to room temperature.

2.4 Synthesis of Ni-NC/MC

0.3 g of NCDs was dissolved in 2 ml of H_2O, then, 0.27 g of nickel nitrate hexahydrate was added, and sonicated for 2 hours to form solution A. 0.2 g of F127 was dissolved in 3 ml of ethanol (1:1) to form solution B. Solutions A and B were mixed to form a clear and transparent yellow-green solution. The mixed solution was added to the culture dishes. After evaporating the solvent at room temperature, the samples were further dried at 60 °C overnight. The final nickel-loaded porous carbon material was obtained by calcination in Ar atmosphere (room temperature-500℃: 2℃ min^{-1}, 500-600℃: 5℃ min^{-1}, 600℃: 3 h).

2.5 Synthesis of Ni-NC/C

0.3 g of NCDs were dissolved in 2 ml of H_2O, then, 0.27 g of nickel nitrate hexahydrate was added, and sonicated for 2 h to form solution A. The solution was poured into a Petri dish, the solvent was evaporated at room temperature, and dried at 60℃ overnight. The resulting nickel-supported carbon material was obtained by calcination under an Ar atmosphere (room temperature-500℃: 2 ℃ min^{-1}, 500-600℃: 5℃ min^{-1}, 600℃: 3 h).

2.6 Synthesis of Ni-NP/MC

0.3 g of NCDs were dissolved in 2 ml of H_2O and sonicated for 2 h to give solution A. 0.2 g of F127 was dissolved in 3 ml of ethanol in water (1:1) to form solution B. Solutions A and B were mixed to give a clear and transparent yellow solution. The mixed solution was poured into a Petri dish, the solvent evaporated at room temperature, and dried overnight at 60℃. The resulting porous carbon material is obtained by calcination under an Ar atmosphere (room temperature-500℃: 2℃ min^{-1}, 500-600℃: 5℃ min^{-1}, 600℃: 3 h). 0.27 g of nickel nitrate hexahydrate was dissolved in 5 ml of H_2O, then, 0.3 g of porous carbon was added and sonicated for 2 h. The mixed solution was poured into the culture dishes. After evaporation of the solvent at room temperature,

the samples were further dried overnight at 60°C. The subsequent calcination conditions were kept unchanged.

2.7 Electrochemical measurements

The HER test was performed on a CHI660E workstation at room temperature and atmospheric pressure. Electrochemical measurements were performed using a typical three-electrode system with a glassy carbon electrode as the working electrode, Hg/HgO as the reference electrode, and a graphitic carbon rod as the counter electrode. To prepare the working electrode, 3 mg of the prepared catalyst was mixed with 500 μL of ethanol and 50 μL of Nafion, then the suspension was ultrasonicated for 20 min and 10 μL of printing ink was dropped onto the glassy carbon electrode (electrode diameter D=5 mm). The solvent was evaporated at room temperature, and the loading amount was 0.28 mg cm^{-2}. The LSV curve was performed with a scan rate of 5 mV s^{-1} in 1 M KOH. The EIS tests were performed with an amplitude of 0.01 V AC and a frequency range of 0.01 to 10^5 Hz. The long-term stability of the catalysts has been evaluated utilizing timed potential measurements. The determination of Cdl is calculated by measuring CV curves at different scan rates (20, 40, 60, 80, and 100 mV s^{-1}). To report the HER measurements, the Hg/HgO electrode was calibrated to a reversible hydrogen electrode (RHE) in an H_2-saturated electrode solution.

$$E_{(RHE)} = E_{(Hg/HgO)} + 0.0592\ pH + 0.098$$

3 Results and discussion

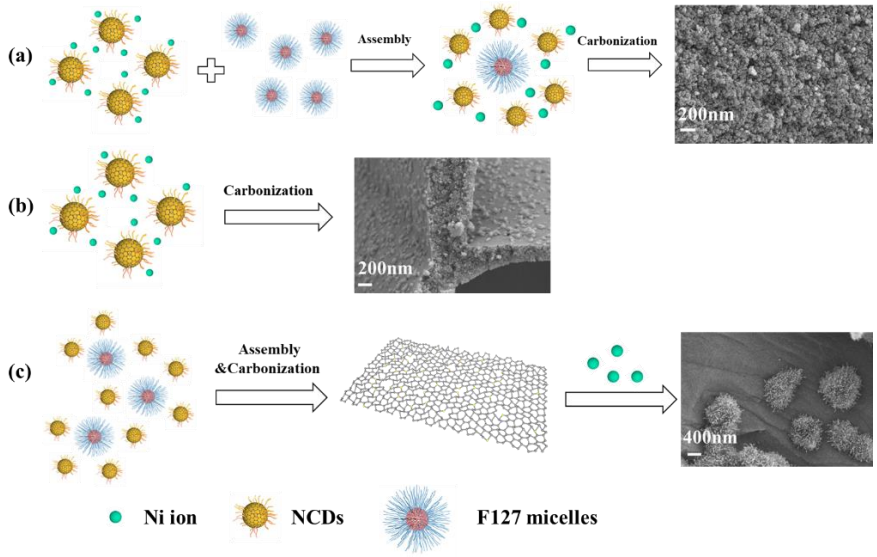

Fig. 1. Schematic illustration for the preparation process of the Ni-NC/MC (a); Ni-NC/C (b); and Ni-NP /MC (c).

The formation process of the composite materials is shown in Fig. 1. Nitrogen-doped carbon dots (NCDs) were prepared by hydrothermal treatment of anhydrous citric acid and L-tryptophan. The surface of the carbon dots (as shown in Fig. 1a) is rich in functional groups that can be chelated with metal ions and then assembled with surfactant F127 to form a mesoporous carbon material loaded with metal and its oxides (denoted as Ni-NC/MC). For comparison, as shown in Fig. 1b, metal-loaded stacked carbon with metals (denoted as Ni-NC/C) were obtained by a similar preparation process to Ni-NC/MC, but without F127. Another comparative sample, denoted as Ni-NP/MC, was prepared by the post-impregnation method, as shown in Fig. 1c. Firstly, NCDs and F127 were assembled and calcined to obtain mesoporous carbon materials, and then metal particles loaded on the mesoporous carbon substrate were obtained by impregnation and calcination.

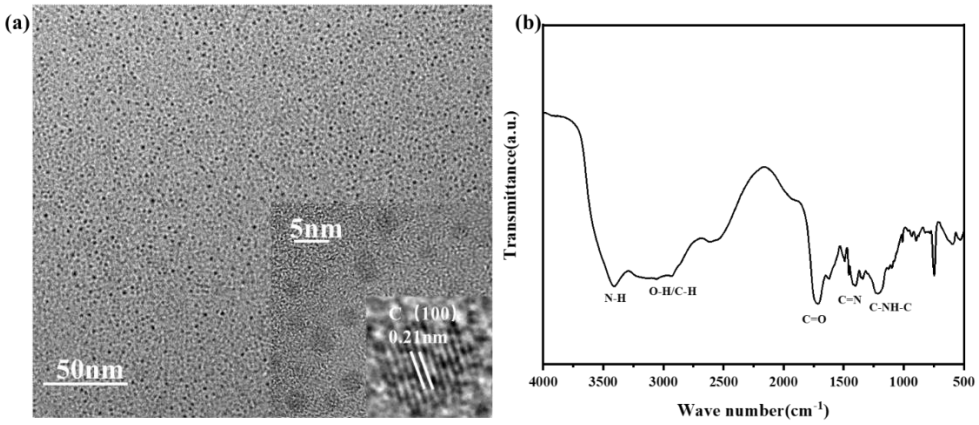

Fig. 2. TEM (a) and FT-IR (b) of NCDs.

The transmission electron microscopy images of NCDs (Fig. 2a) display a spherical morphology with a diameter of approximately 3 nm. The HRTEM image reveals a distinct lattice structure with a crystal plane spacing of 0.21 nm, corresponding to the (100) crystal faces of graphitic carbon. The Fourier transform infrared spectrometer (FT-IR) of NCDs (Fig. 2b) displays the bending vibration of N-H at 3415 cm^{-1}, the telescopic vibration of O-H at 3019 cm^{-1}, the vibration absorption of C=O at 1719 cm^{-1}, the telescopic vibration of C=N at 1410 cm^{-1}, and the asymmetric telescopic

vibration of C-NH-C at 1216 cm^{-1}.[25, 26]

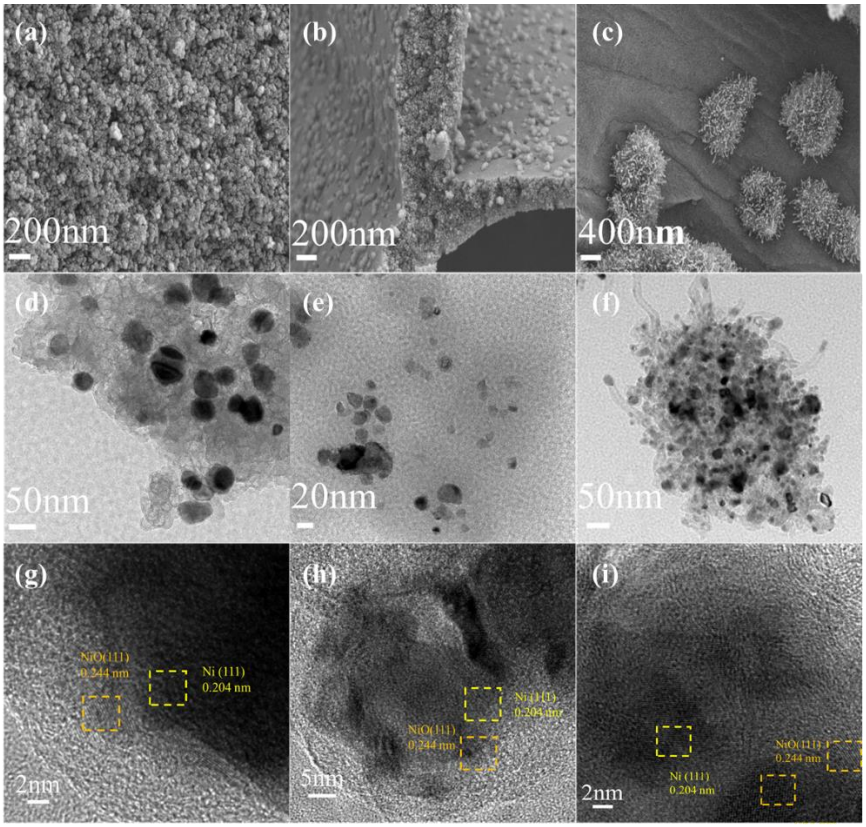

Fig. 3. SEM images of Ni-NC/MC (a), Ni-NC/C (b), Ni-NP/MC (c); TEM images of Ni-NC/MC (d), Ni-NC/C (e), Ni-NP/MC (f), and HRTEM of Ni-NC/MC (g), Ni-NC/C (h), Ni-NP/MC (i).

The scanning electron microscope (SEM) images of the Ni-NC/MC catalyst (Fig. 3a) reveal a nanoparticle-like morphology. Conversely, the Ni-NC/C catalyst synthesized without the addition of surfactant F127 exhibits an overall lamellar structure with nanoparticles embedded nanoparticles (Fig. 3b). The SEM image of the Ni-NP/MC catalyst shows that the spiny spherical metal and its oxides are distributed on the smooth carbon substrate (Fig. 3c). The TEM images of the catalysts Ni-NC/MC and Ni-NC/C (Fig. 3d, e) show an average metal particle size of 20 nm. Compared to the Ni-NC/C catalyst, the addition of surfactant F127 to the assembly process resulted in more hollow structures in the carbon substrate of the Ni-NC/MC catalyst. Fig. 3f shows that due to the "tip growth mode"[27], some carbon nanotubes and internal metal particles can be observed in Ni-NP/MC. The metal salt solution is pyrolyzed into metal and its oxides at high temperatures after impregnation and loading onto the surface of the carbon material. The average particle size is approximately 40 nm. The catalyst's

HRTEM (Fig. 3g-i) reveals the positional relationship and crystal plane information of the metal and its oxide, specifically the 111 crystal plane of nickel (0.204 nm) and the 111 crystal plane of nickel oxide (0.245 nm).[28] The catalyst EDS is shown in Figure S1 (EDS), displaying the distribution of four elements: C, Ni, O, and N. The surface of the catalyst exhibits a heterostructure of Ni/NiO, with nickel metal primarily coordinated with nitrogen and oxygen.

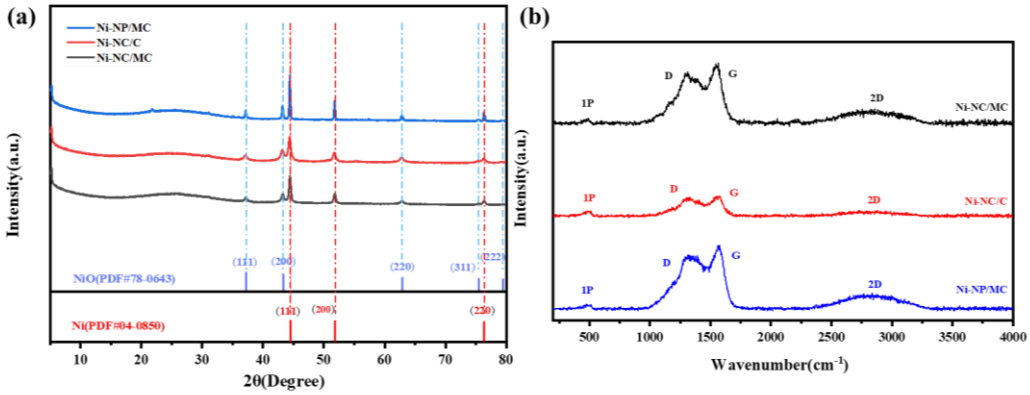

Fig. 4. XRD patterns (a) and Raman spectra (b) of the catalysts.

The corresponding information for the composite is shown in Fig. 4a. The wide and weak peak at 25° is attributed to the typical peak (002) of carbon, indicating that the composite has weak graphitization characteristics. The peaks at 44.3°, 51.6° and 76.1° correspond to the (111), (200) and (220) crystal planes of the cubic nickel phase (JCPDS No.04-0850)[29]. The peaks at 37.1°, 43.1°, 62.7°, 75.1° and 79.3° are attributed to the (111), (200), (220), (311) and (222) crystal planes of nickel oxide (JCPDS No.78-0643). It can be seen that the metal in the composite material mainly exists in the form of metal and its oxide. The grain size of each catalyst can be determined by calculating the strongest peaks of the (Ni-NC /MC, Ni-NC/C, and Ni-NP/MC) catalysts, specifically the half-peak width of the Ni (111) crystal plane and the NiO (200) crystal planes. Among them, the Ni-NC/MC nickel catalyst has a grain size of 25 nm for nickel and 17 nm for nickel oxide. The Ni-NC/C catalyst has a grain size of 19 nm for nickel and 13 nm for nickel oxide. The Ni-NP/MC catalyst has a grain size of 40 nm for nickel and 25 nm for nickel oxide. The addition of surfactant F127 does not affect the particle size of the metal, and the carbon dots play a certain limiting role, thereby avoiding

further growth of the particle size. This is demonstrated by the Raman spectrum of the catalyst in Fig. 4b. The catalyst's peaks at 1320 cm^{-1} and 1560 cm^{-1} are attributed to the D band peak and G band peak of carbon, respectively. The former corresponds to defects in sp^2 hybrid carbon, while the latter corresponds to ordered graphite.[30] The D/G band integral area ratio of the Ni-NC/MC catalyst is 2.05 (Ni-NC/C: 1.25, Ni-NP/MC: 1.59), indicating a higher degree of structural defect. The catalyst's cubic structure contains a single-atom primordial unit cell of metal nickel. As a result, Ni does not show any peaks in Raman spectroscopy, nor does it show any variation in polarizability due to the interaction between the electric field of monochromatic light and the dipole moment within the material.[31] The catalyst's peak value around 490 cm^{-1} corresponds to NiO-phonon (1p) longitudinal optics (LO).[32] The medium-wide 2D peak near 2700 cm^{-1} can be attributed to the multilayer graphite in the catalyst, which is consistent with the observation in TEM, which is beneficial to improve the conductivity of the material, accelerate the electron transfer rate, and improve the electrochemistry of the catalyst. The difference in Raman intensity between Ni-NC/MC and Ni-NC/C can be attributed to the addition of surfactants. The incomplete calcination of F127 increases the content of carbon and defects, which may affect the surface chemical properties of the material and be beneficial to the improvement of catalyst performance.

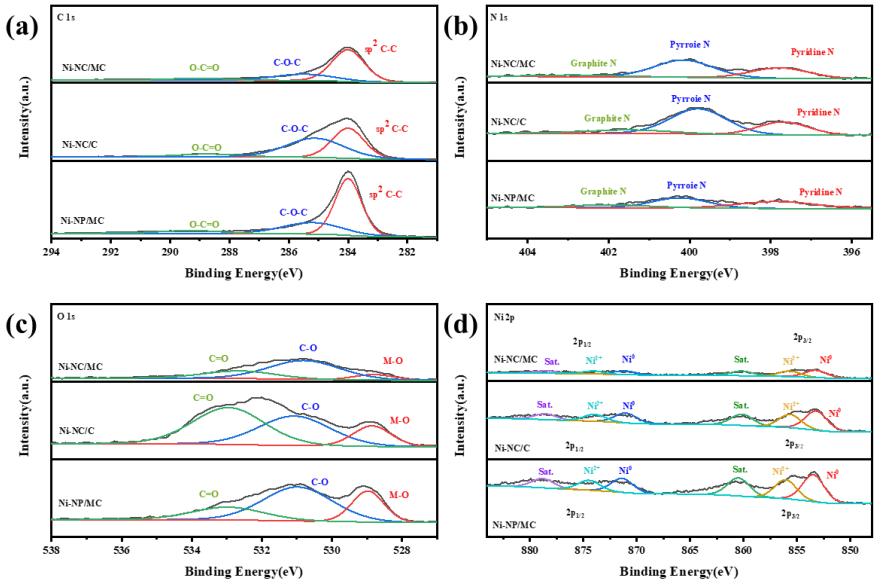

Fig. 5. Structural characterization of composites C1s spectra (a); N1s spectrum (b); O1s spectrum

(c); Ni 2p spectrum (d).

The bonding state and surface chemical composition of the catalyst samples were characterized by XPS. All the catalysts contain four elements, C, N, O, and Ni. As shown in Fig. 5a, three characteristic peaks in the C1s spectra of Ni-NC / MC catalyst can be attributed to sp^2 C-C (284 eV), C-O-C (285.48 eV) and O-C=O (289 eV). The characteristic peaks of C1s for the Ni-NC/C and Ni-NP/MC catalysts are consistent, but the peak position is shifted. Compared to the Ni-NC/MC catalyst, the peak positions of the C-O-C and O-C=O bonds in the catalyst Ni-NC/C assembled without surfactants shifted to lower binding energy positions by 0.37 and 0.28 eV, respectively. The position of the C-O-C bond peak of the Ni-NP/MC catalyst shifted towards lower binding energy by 0.26 eV. Similarly, the peak position of the O-C=O bond shifted towards higher binding energy by 0.28 eV. These observations suggest that the carbon in the Ni-NC/MC catalyst transfers electrons outward. As shown in fig. 5b, the characteristic peaks of the catalyst near 397.8 eV, 400.1 eV and 402 eV, which correspond to pyridine nitrogen, pyrrole nitrogen and graphite nitrogen, respectively. The peak positions of the samples without surfactants towards the low binding energy direction, with the specific values of 0.09, 0.36 and 1.42 eV, respectively. The peak positions of pyridine nitrogen and pyrrole nitrogen in the Ni-NP/MC catalyst with the confinement effect are shifted by 0.06 and 0.09 eV towards high binding energy, respectively. Similarly, the peak position of graphite nitrogen is shifted by 0.93 eV towards low binding energy, indicating that the nitrogen in the carbon substrate gains electrons. Fig. 5c shows the O1s spectra of the catalyst. The Ni-NC/MC catalyst exhibits a characteristic peak at 528.8 eV is attributed to M-O, another at 530.79 eV attributed to C-O, and a third at 532.64 eV attributed to C=O. The characteristic peak positions of the Ni-NC/C catalyst assembled without surfactants are shifted towards higher binding energy by 0.05, 0.72, and 0.31 eV, respectively. The characteristic peak positions of the Ni-NP/MC catalyst exploring the confinement effect of carbon dots are shifted to the high binding energy by 0.17, 0.18, and 0.33 eV, respectively, indicating that the oxygen in the surfactant obtains a lot of electrons, which is complementary to the offset of the carbon peak, indicating that the surfactant mainly acts on the carbon-oxygen bond. The Ni 2p XPS

spectrum of the catalyst is shown in Fig. 5d. Due to the influence of spin-orbit, the peak of Ni 2p is mainly composed of Ni $2p_{1/2}$ and Ni $2p_{3/2}$. For the Ni-NC/MC catalyst, the peaks at 853.26 and 871.19 eV can be attributed to the $2p_{3/2}$ and $2p_{1/2}$ orbitals of the metal nickel. The peaks at 855.69 and 874.1 eV can be attributed to the $2p_{3/2}$ and $2p_{1/2}$ orbitals of nickel oxide. The results show that the metal in the catalyst is in the form of metal and its oxide, which is consistent with the XRD results. The peaks at 860.16 and 878.47 eV are satellite peaks. In addition, according to the peak area of XPS, the mass ratio of Ni/NiO in the catalyst is 1.3: 1. For the Ni-NC/C catalyst, the peaks at 853.22 and 871.04 eV can be attributed to the $2p_{3/2}$ and $2p_{1/2}$ orbitals of the metal nickel. The peaks at 855.66 and 873.94 eV can be attributed to the $2p_{3/2}$ and $2p_{1/2}$ orbitals of nickel oxide, and the peaks at 860.16 and 878.56 eV are satellite peaks. According to the peak area of XPS, the mass ratio of Ni/NiO in the catalyst is 1.45: 1. For the catalyst Ni-NP/MC, the peaks at 853.48 and 871.37 eV can be attributed to the $2p_{3/2}$ and $2p_{1/2}$ orbitals of nickel. The peaks at 856.07 and 874.48 eV can be attributed to the $2p_{3/2}$ and $2p_{1/2}$ orbitals of nickel oxide, and the peaks at 860.50 and 878.81eV are satellite peaks. According to the XPS peak area, the mass ratio of Ni/NiO in the catalyst is 1.42: 1. The metal peak position of the catalyst has shifted to a higher binding energy position, possibly due to the charge transfer from the metal nanoparticles to the graphitic carbon layer.[27] In addition, the metal peak position of catalysts Ni-NC/MC and Ni-NC/C remained almost unchanged, indicating that the surfactant did not affect the metal bonding.

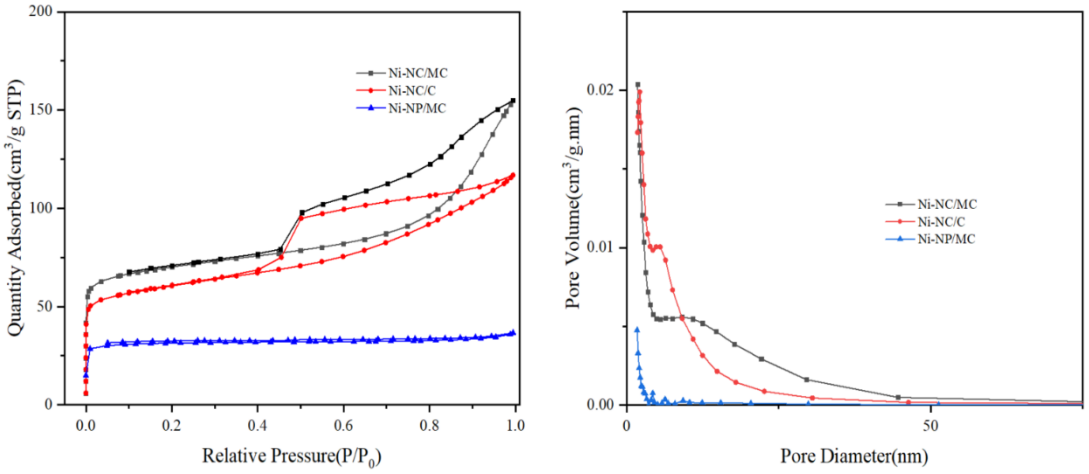

Fig. 6. Nitrogen adsorption-desorption curve and pore size distribution.

Fig. 6 shows the nitrogen adsorption-desorption isotherms and pore size distribution of the composite materials. Both catalysts, Ni-NC/MC and Ni-NC/C exhibited type IV adsorption isotherms, indicating the presence of mesopores in the samples. The adsorption isotherm of the sample after impregnation (Ni-NP/MC) is type I, which belongs to the microporous isotherm. The TEM (Fig. S2) of the calcined catalyst precursor assembled by carbon dots and surfactants showed irregular pores. This may be due to the assembly of surfactant F127 around the functional groups on the surface of carbon dots. The BET table is shown in Fig. S3. The data presented shows the specific surface area and pore structure of the catalyst sample. The post-impregnated sample has the smallest specific surface area (125 $m^2 g^{-1}$). A larger specific surface area and pore size are conducive to the exposure of more active sites and the transport of substances in the catalytic process to achieve higher electrocatalytic performance.

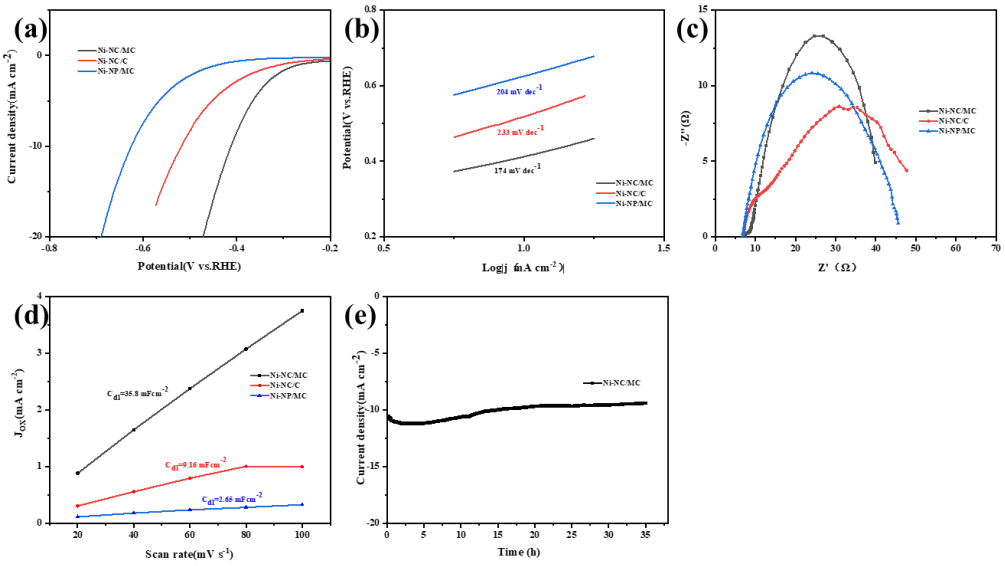

Fig. 7. HER performance of catalyst LSV curves (a); Tafel slope (b); Nyquist curves (c); double-layer capacitance (Cdl) (d); i-t curves (e).

The electrocatalytic performance of the catalysts for HER was compared in an alkaline medium (1 M KOH, pH = 13.8). Fig. 7a shows the linear sweep voltammetry curve. The catalyst Ni-NC/MC exhibited better performance than the sample without surfactant (Ni-NC/C) and the sample impregnated with metal (Ni-NP/MC). This may be attributed to the large specific surface area and pore size resulting from the assembly of surfactant F127 and the size effect of the carbon dots themselves. The Tafel slope of

the catalyst is obtained by the Tafel equation ($\eta = b \log (j) + a$). Here η represents the overpotential, j represents the current density, and b represents the Tafel slope, which can be popularly understood as the overpotential required for the current density to increase by an order of magnitude. Therefore, a smaller Tafel slope (b value) indicates a faster kinetic process. In alkaline media, the HER reaction involves three fundamental reactions[33] :

$$H_2O + e^- + M \rightarrow M\text{-}H_{ads} + OH^- \text{ (Volmer reaction，120 mV dec}^{-1}\text{)}$$

$$M\text{-}H_{ads} + M\text{-}H_{ads} \rightarrow 2\ M + H_2 \text{ (Tafel reaction，30 mV dec}^{-1}\text{)}$$

$$M\text{-}H_{ads} + H_2O + e^- \rightarrow M + H_2 + OH^- \text{ (Heyrovsky reaction，40 mV dec}^{-1}\text{）}$$

The Tafel values of the catalysts were all greater than 120 mV dec^{-1}, indicating that the Volmer step was the rate-determining step, which further indicated that OH^- adsorption at the catalytic site was relatively weak. The information on internal resistance and material conductivity can be obtained by electrochemical impedance test. A smaller semicircle diameter indicates faster charge transfer and better conductivity of the catalyst. Therefore, it can be seen from Fig. 7c that Ni-NC/MC has the best conductivity. The size of the bilayer capacitance Cdl responds to the size of the catalyst active area ECSA, Cdl values can be obtained from cyclic voltammetric curves at different sweep speeds. The larger the Cdl value, the larger the active area and the more active components. The Cdl of Ni-NC/MC is 35.8 mF cm^{-2}, significantly higher than that of Ni-NC/C (9.16 mF cm^{-2}) and Ni-NP/MC (2.65 mF cm^{-2}). Stabilized by constant voltage tested (Fig. 7e), the catalyst has good stability.

According to the research results, the performance sources of the catalyst are mainly as follows: Firstly, on the Ni/NiO heterostructure interface, due to the electrostatic adsorption capacity of Ni^{2+} and more unfilled d orbitals than Ni, OH^- generated by H_2O cracking is more easily adsorbed on the NiO interface, and the nearby Ni is beneficial to the adsorption of H, thus promoting the Volmer reaction.[34] Secondly, the addition of surfactants provides a more specific surface area for the active site, provides more pores for the transport of substances during the reaction, provides more defects, and coordinates the surface chemical state of the material. Finally, the carbon core derived from its characteristics plays a role in confinement to a certain extent,

thereby inhibiting the further growth of metals. In the heterogeneous structure of Ni/NiO, the ratio of Ni/NiO also affects the HER performance to some extent.[13]

4 Conclusion

In summary, mesoporous carbon materials loaded with Ni/NiO heterostructure were successfully synthesized by co-assembling surfactants with metal ions and nitrogen-doped carbon dots. the catalytic performance of the basic HER was verified due to the increased specific surface area and the domain-limiting effect of the carbon sites brought by the surfactant. The overpotential values of the catalyst Ni-NC/MC were about 100 mV and 210 mV lower compared to the sample without surfactant addition (Ni-NC/C) and the metal post-impregnation loaded sample (Ni-NP/MC), respectively. The performance of the catalyst comes from the heterostructure of Ni/NiO. In addition, the right Ni/NiO ratio is also beneficial to HER. Our results provide certain parameters for carbon source selection for the preparation of mesoporous carbon by carbon dot size effect and soft template method.

Acknowledgements

This work was financially supported by the National Natural Science Foundation of China (No. U21A20329). The authors express thanks to the Advanced Analysis and Gene Sequencing Center of Zhengzhou University for their support in materials characterization.

References

[1] LAI W H, ZHANG L F, HUA W B, et al. General pi-Electron-Assisted Strategy for Ir, Pt, Ru, Pd, Fe, Ni Single-Atom Electrocatalysts with Bifunctional Active Sites for Highly Efficient Water Splitting [J]. Angew Chem Int Ed Engl, 2019, 58(34): 11868-73.

[2] DENG Y, LAI W, XU B. A Mini Review on Doped Nickel-Based Electrocatalysts for Hydrogen Evolution Reaction [J]. Energies, 2020, 13(18): 4651.

[3] LI D, SHI J, LI C. Transition-Metal-Based Electrocatalysts as Cocatalysts for Photoelectrochemical Water Splitting: A Mini Review [J]. Small, 2018, 14(23): e1704179.

[4] ZHANG Q, GUAN J. Single-Atom Catalysts for Electrocatalytic Applications [J]. Advanced

Functional Materials, 2020, 30(31): 2000768.

[5] ZHOU Z, PEI Z, WEI L, et al. Electrocatalytic hydrogen evolution under neutral pH conditions: current understandings, recent advances, and future prospects [J]. Energy & Environmental Science, 2020, 13(10): 3185-206.

[6] YANG W, CHEN S. Recent progress in electrode fabrication for electrocatalytic hydrogen evolution reaction: A mini review [J]. Chemical Engineering Journal, 2020, 393: 124726.

[7] LI C, BAEK J B. Recent Advances in Noble Metal (Pt, Ru, and Ir)-Based Electrocatalysts for Efficient Hydrogen Evolution Reaction [J]. ACS Omega, 2020, 5(1): 31-40.

[8] WU H, FENG C, ZHANG L, et al. Non-noble Metal Electrocatalysts for the Hydrogen Evolution Reaction in Water Electrolysis [J]. Electrochemical Energy Reviews, 2021, 4(3): 473-507.

[9] ZHANG X-Y, XIE J-Y, MA Y, et al. An overview of the active sites in transition metal electrocatalysts and their practical activity for hydrogen evolution reaction [J]. Chemical Engineering Journal, 2022, 430: 132312.

[10] ESPOSITO D V, HUNT S T, KIMMEL Y C, et al. A new class of electrocatalysts for hydrogen production from water electrolysis: metal monolayers supported on low-cost transition metal carbides [J]. J Am Chem Soc, 2012, 134(6): 3025-33.

[11] LEI C, WANG Y, HOU Y, et al. Efficient alkaline hydrogen evolution on atomically dispersed Ni–Nx Species anchored porous carbon with embedded Ni nanoparticles by accelerating water dissociation kinetics [J]. Energy & Environmental Science, 2019, 12(1): 149-56.

[12] YAN X, GU M, WANG Y, et al. In-situ growth of Ni nanoparticle-encapsulated N-doped carbon nanotubes on carbon nanorods for efficient hydrogen evolution electrocatalysis [J]. Nano Research, 2020, 13(4): 975-82.

[13] HAN H, PARK S, JANG D, et al. N-doped carbon nanoweb-supported Ni/NiO heterostructure as hybrid catalysts for hydrogen evolution reaction in an alkaline phase [J]. Journal of Alloys and Compounds, 2021, 853: 157338.

[14] JIN H, LIU X, CHEN S, et al. Heteroatom-Doped Transition Metal Electrocatalysts for Hydrogen Evolution Reaction [J]. ACS Energy Letters, 2019, 4(4): 805-10.

[15] GAO D, LIU R, BISKUPEK J, et al. Modular Design of Noble-Metal-Free Mixed Metal Oxide Electrocatalysts for Complete Water Splitting [J]. Angew Chem Int Ed Engl, 2019, 58(14):

4644-8.

[16] ZHANG L, XIAO J, WANG H, et al. Carbon-Based Electrocatalysts for Hydrogen and Oxygen Evolution Reactions [J]. ACS Catalysis, 2017, 7(11): 7855-65.

[17] DUAN J, CHEN S, JARONIEC M, et al. Porous C_3N_4 nanolayers@n-graphene films as catalyst electrodes for highly efficient hydrogen evolution [J]. Acs Nano, 2015, 9(1): 931-40.

[18] CHENG X-F, HE J-H, JI H-Q, et al. Coordination Symmetry Breaking of Single-Atom Catalysts for Robust and Efficient Nitrate Electroreduction to Ammonia [J]. Advanced Materials, 2022, 34(36): 2205767.

[19] SONG H, WU M, TANG Z, et al. Single Atom Ruthenium-Doped CoP/CDs Nanosheets via Splicing of Carbon-Dots for Robust Hydrogen Production [J]. Angew Chem Int Ed Engl, 2021, 60(13): 7234-44.

[20] SONG H, YU J, TANG Z, et al. Halogen-Doped Carbon Dots on Amorphous Cobalt Phosphide as Robust Electrocatalysts for Overall Water Splitting [J]. Advanced Energy Materials, 2022, 12(14): 2102573.

[21] HONG Q, WANG Y, WANG R, et al. In Situ Coupling of Carbon Dots with Co-ZIF Nanoarrays Enabling Highly Efficient Oxygen Evolution Electrocatalysis [J]. Small, 2023, 19(31): 2206723.

[22] JI Z, LIU K, LI N, et al. Nitrogen-doped carbon dots anchored NiO/Co₃O₄ ultrathin nanosheets as advanced cathodes for hybrid supercapacitors [J]. Journal of Colloid and Interface Science, 2020, 579: 282-9.

[23] WANG Z, LIU C-J. Preparation and application of iron oxide/graphene based composites for electrochemical energy storage and energy conversion devices: Current status and perspective [J]. Nano Energy, 2015, 11: 277-93.

[24] HUANG X, LI J, XIN Z. Serrin-Type Criterion for the Three-Dimensional Viscous Compressible Flows [J]. SIAM Journal on Mathematical Analysis, 2011, 43(4): 1872-86.

[25] ZHANG S, GAO M, ZHAI Y, et al. Which kind of nitrogen chemical states doped carbon dots loaded by g-C(3)N(4) is the best for photocatalytic hydrogen production [J]. J Colloid Interface Sci, 2022, 622: 662-74.

[26] SONG H, CHENG Y, LI B, et al. Carbon Dots and RuP2 Nanohybrid as an Efficient Bifunctional Catalyst for Electrochemical Hydrogen Evolution Reaction and Hydrolysis of

Ammonia Borane [J]. ACS Sustainable Chemistry & Engineering, 2020, 8(9): 3995-4002.

[27] CHENG N, WANG N, REN L, et al. In-situ grafting of N-doped carbon nanotubes with Ni encapsulation onto MOF-derived hierarchical hybrids for efficient electrocatalytic hydrogen evolution [J]. Carbon, 2020, 163: 178-85.

[28] ZHOU W, LU X F, CHEN J J, et al. Hierarchical Porous Prism Arrays Composed of Hybrid Ni-NiO-Carbon as Highly Efficient Electrocatalysts for Overall Water Splitting [J]. ACS Appl Mater Interfaces, 2018, 10(45): 38906-14.

[29] HE F, WANG Y, ZHONG M, et al. Construction of nickel nanoparticles embedded in nitrogen self-doped graphene-like carbon derived from waste grapefruit peel for multifunctional OER, HER, and magnetism investigations [J]. Journal of Environmental Chemical Engineering, 2021, 9(6): 106894.

[30] YAN Y, MA Q, CUI F, et al. Carbon onions coated Ni/NiO nanoparticles as catalysts for alkaline hydrogen evolution reaction [J]. Electrochimica Acta, 2022, 430: 141090.

[31] KWAN J T H, BONAKDARPOUR A, AFONSO G, et al. Bridging Fundamental Electrochemistry with Applied Fuel Cell Testing: A Novel and Economical Rotating Disk Electrode Tip for Electrochemical Assessment of Catalyst-Coated Membranes [J]. Electrochimica Acta, 2017, 258: 208-19.

[32] MIRONOVA-ULMANE N, KUZMIN A, STEINS I, et al. Raman scattering in nanosized nickel oxide NiO [J]. Journal of Physics: Conference Series, 2007, 93: 012039.

[33] CHEN J, JIA J, WEI Z, et al. Ni and N co-doped MoCx as efficient electrocatalysts for hydrogen evolution reaction at all-pH values [J]. International Journal of Hydrogen Energy, 2018, 43(31): 14301-9.

[34] GONG M, ZHOU W, KENNEY M J, et al. Blending Cr2O3 into a NiO-Ni electrocatalyst for sustained water splitting [J]. Angew Chem Int Ed Engl, 2015, 54(41): 11989-93.